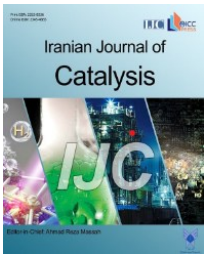

Iran. J. Catal. 2026; 16(2): 265-283

Iranian Journal of Catalysis (IJC)

https://doi.org/10.57647/ijc.2026.1602.17

Research Article

Optimization of Enhanced Photocatalytic Degradation of Turquoise Blue G (TBG) Using a Cu-N:ZnO/TiO_2 Nano-Heterojunction Photocatalyst via Response Surface Methodology (RSM)

Mangesh K. Lanjewar[1,2], Omprakash K. Mahadwad[3,*], Pritam Patil[4]

[1]*Research Scholar, Gujarat Technological University, Ahmedabad 382424, India*
[2]*Department of Chemical Engineering, Government Engineering College, Bharuch 392001, India*
[3]*Department of Chemical Technology, UPL University of Sustainable Technology, Ankleshwar 393135, India*
[4]*Department of Chemical Engineering, Shri S'ad Vidya Mandal Institute of Technology, Bharuch 392001, India*

*Corresponding authors: omprakash.mahadwad@upluniversity.ac.in

Article History:

Received:
01 January 2026

Revised:
07 February 2026

Accepted:
03 March 2026

Published Online:
08 May 2026

Published in Issue:
30 June 2026

Abstract

A novel Cu-N co-doped ZnO/TiO_2 (7% Cu-N:ZnO/TiO_2) modified Type-II nano-heterojunction photocatalyst was synthesized using a cost-effective room temperature sol-gel (RTSG) method to enhance dye degradation performance. Nitrogen doping levels (1-5 wt%) were optimized relative to the 7% Cu doped ZnO/TiO_2 system. Structural, morphological, optical, and surface chemical properties were systematically characterized using XRD, FE-SEM, UV-Vis, XPS and FTIR. Among all, the 3 wt% N-doped catalyst, 7% Cu-N(3%):ZnO/TiO_2, exhibited the significant red shift (388.71 → 417.5 nm) and notable band-gap reduction from 3.19 eV (pure TiO_2) to 2.97 eV, enabling superior visible-light absorption. For the first time, this optimized photocatalyst was applied for the photocatalytic degradation of Turquoise Blue G (TBG) dye, achieving an excellent degradation efficiency of 98.07% within 150 minutes-1.57 times higher than pure TiO_2 and reducing COD to a level 5.5 times lower than untreated wastewater, confirming effective mineralization. Compared with our earlier Cu doped ZnO/TiO_2 system, nitrogen incorporation further enhanced charge separation and reaction kinetics. Additionally, RSM using Central Composite Design (CCD) was employed to model, analyze, and optimize key process parameters, showing strong predictive accuracy. This study demonstrates that Cu-N co-doping provides a highly efficient and scalable strategy for sustainable photocatalytic treatment of dye wastewater.

Keywords: Modified type II heterojunction; Photocatalytic degradation; RSM-CCD, Sol-gel method; Turquoise blue G (TBG) dye

Cite this article: M. K. Lanjewar, O. K. Mahadwad, P. Patil, Iran. J. Catal. **16** (2026) 265-283. https://doi.org/10.57647/ijc.2026.1602.17

1. Introduction

The escalating contamination of water sources by industrial effluents especially from textile, paper, and plastic industries, poses serious threats to aquatic ecosystems and human health [1,2]. Synthetic dyes are a key pollutant in these effluents, and due to their complex aromatic structures and stability, they often resist conventional physical and biological treatments [3]. These dyes can impair photosynthesis in aquatic

organisms and may be toxic, mutagenic, or carcinogenic even at low concentrations [4]. Therefore, developing efficient, sustainable, and low-cost strategies for complete dye degradation is critically important. Advanced oxidation processes (AOPs) now evolved into highly effective treatment technologies to degrade dyes via the generation of reactive hydroxyl radicals (· OH), which mineralise organic pollutants into harmless CO_2 and H_2O [5]. Among various AOPs, heterogeneous photocatalysis using solar-activated semiconductor materials has gained attention due to ambient operation and scalability [6,7].

Zinc oxide (ZnO) and titanium dioxide (TiO_2) are among the most extensively investigated photocatalysts, due to their high reactivity, non-toxicity, chemical stability, and low cost [8]. However, their wide band gaps (approximately 3.0-3.2 eV for TiO_2 anatase and 3.37 eV for pure ZnO) restrict activation to the UV region (~4% of solar spectrum), and their rapid electron-hole recombination lowers photocatalytic efficiency [9].

To address these issues, researchers have developed semiconductor heterojunctions that improve charge separation via staggered band structures [10]. Notably, TiO_2-ZnO heterostructures have shown improved visible-light absorption and enhanced photocatalytic activity due to efficient interfacial charge transfer [11].

Moreover, non-metal doping (e.g., nitrogen) can introduce mid-gap states and narrow the band gap, enabling visible-light responsiveness [12,13], while metal dopants such as copper serve as electron traps that further enhance charge separation [14,15]. Co-doping with both nitrogen and copper in TiO_2-ZnO heterostructures creates synergistic improvements in light absorption and carrier dynamics, surpassing the effects of individual dopants [10,16].

For practical application, turquoise blue dyes-commonly used in textiles are recalcitrant and difficult to degrade under visible light. Thus, our study centered on synthesis of a copper and nitrogen co-doped ZnO-TiO_2 heterojunction photocatalyst to achieve improved photocatalytic degradation of TBG by analyzing its optical, structural, and photocatalytic characteristics.

Enhancing the efficiency of heterojunction photocatalysts is essential for advancing applications in environmental remediation and solar energy conversion. Since several effective parameters like pH, catalyst dosage, dopant concentration, and irradiation time play interdependent roles, unlike traditional one-factor-at-a-time (OFAT) optimization, which varies only one parameter while holding others constant, the design of experiments (DoE) approach such as response surface methodology (RSM) enables a systematic and statistically robust investigation of multiple factors simultaneously. This allows for efficient exploration of interaction effects between variables that OFAT cannot detect, providing a more comprehensive understanding of the process behavior. DoE also significantly improves experimental efficiency by reducing the total number of experimental runs required to achieve reliable optimization results, saving time and resources. Moreover, DoE provides quantitative models that can predict system responses across the experimental domain, whereas OFAT methods often yield only local optima and overlook interaction and curvature effects. Therefore, DoE/RSM offers superior optimization capability, deeper mechanistic insight and better predictive accuracy compared to OFAT approaches in multi-parameter process optimization studies [17,18]. RSM along with Central Composite Design (CCD) offers a streamlined and statistically robust approach to model such multifactorial systems. CCD enables the development of second-order polynomial models that account for linear, quadratic, and interaction effects, while minimizing the number of experimental runs. This methodology has been successfully applied for optimizing photocatalytic degradation processes [19,20]. Building on these precedents, the present study applies RSM-CCD to a Cu-N co-doped ZnO/ TiO_2 heterojunction to systematically explore key factors and identify the optimal conditions for improved photocatalytic activity.

The novelty and key advantages of the present work over existing ZnO/TiO_2 based photocatalysts are summarized below. Building upon our earlier work on Cu doped ZnO/TiO_2 Type-II heterojunctions for TBG dye degradation [21], the present study introduces a novel Cu-N co-doped ZnO/TiO_2 modified Type-II heterojunction photocatalyst developed via a modified sol-gel (RTSG) route. While Cu doping alone significantly improved visible-light absorption and photocatalytic activity, the strategic incorporation of nitrogen (1-5 wt%) into the optimized 7% Cu:ZnO/TiO_2 further engineered the electronic structure, yielding a substantially narrowed band gap (2.97 eV) compared to pristine TiO_2 (3.19 eV). This dual doping approach not only enhanced charge separation through a modified Type-II heterojunction but also promoted additional mid-gap states, enabling superior utilization of the visible-light spectrum. As a result, the optimized 7% Cu-N (3%):ZnO/TiO_2 photocatalyst achieved 98.07% for the first time degradation of TBG dye, demonstrating a 1.57-fold improvement over pure TiO_2, along with a remarkable 5.5-fold reduction in COD than that of the untreated wastewater. confirming deeper mineralisation. Moreover, Response Surface Methodology (RSM) using CCD was employed for the first time on this system to statistically optimize key parameters, identify interactive effects, and establish predictive process models. The integration of co-doping, heterojunction engineering, and RSM guided optimization provides a comprehensive and novel framework for designing highly active, reusable, and industrially viable photocatalysts for sustainable dye wastewater treatment.

10.57647/ijc.2026.1602.17

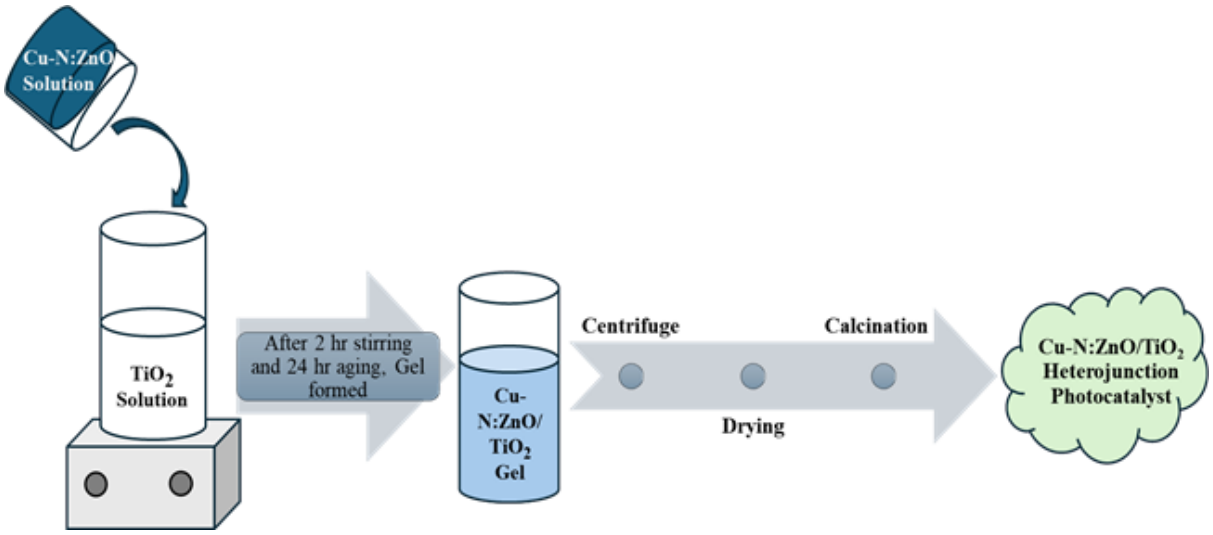

Figure 1. Schematic of Cu-N:ZnO/TiO_2 nano heterojunction photocatalyst synthesis process by sol-gel method

2. Experimental

2.1. Materials

Titanium isopropoxide (TTIP) (99%) and cupric nitrate trihydrate (98%) were sourced from Sisco Research Laboratories Pvt. Ltd., Mumbai, India. Zinc acetate dihydrate (98%) was procured from Loba Chemie Pvt. Ltd., Mumbai, India. Urea extrapure purchased from finar Ltd., Ahmedabad, Gujarat. All chemicals were of analytical grade; they were used without any further purification Experiments were conducted under ambient conditions with distilled water used for preparing all aqueous solutions.

2.2. Cu-N:ZnO/TiO_2 nano heterojunction photocatalyst synthesis via Sol-Gel method

TiO_2 Solution preparation: 0.01 Molar (M) TTIP was added dropwise in 20 mL of ethanol with continuous stirring at 500-600 rpm with the help of magnetic stirrer at ambient condition. 3-5 mL pure acetic acid added dropwise in TTIP solution to maintain pH 3-4 with continuous stirring. A slightly whitish colour solution is observed. Stir the solution for 5-10 minutes at room temperature.

Cu-N:ZnO Solution preparation: 0.01 M of zinc acetate dihydrate added slowly in 20 mL ethanol in another beaker continuously stirring using magnetic stirrer with 400-500 rpm at room temperature. Added 10 mL water dropwise to completely dissolve zinc acetate dihydrate with stirring then added cupric nitrate trihydrate (7 wt% Cu based on ZnO and TiO_2 1:1 molar ratio) slowly while stirring. After completely dissolve cupric nitrate trihydrate added 1wt% - 5wt% nitrogen based on 7% Cu:ZnO/TiO_2 urea extrapure in measured quantity with continuous stirring. After completely dissolve of urea extrapure added 5-10 mL pure acetic acid to maintain pH 3-4 at room temperature. Transparent greenish blue colour solution was prepared.

Cu-N:ZnO/TiO_2 Solution preparation: Added Cu-N:ZnO solution in TiO_2 solution dropwise at room temperature with vigorous stirring by magnetic stirrer. While addition of Cu-N:ZnO solution in TiO_2 solution, viscosity of mixture was increased. During addition of Cu-N:ZnO solution, maintained mixture pH 3-4 by adding acetic acid. Stir the mixture of both solutions for 1h at ambient condition. This resulted greenish blue thick sol and then aged for 24h. After aging for 24h, the gel was formed. To remove impurities, the material was washed with water using a high-speed centrifuge. It was then dried at 100°C for 2h. The dry material was ground and then calcined at 500°C for 2h. Slight greenish fine crystalline heterojunction photocatalyst was synthesized. Diagrammatic representation of Cu-N:ZnO/TiO_2 nano heterojunction photocatalyst synthesis process by sol-gel method shown in Fig. 1. To analyze and correlate the photocatalytic performance, pure TiO_2, pure ZnO, ZnO/TiO_2, and Cu:ZnO/TiO_2 (1 wt% - 9 wt%) were synthesized separately by same methodology [21].

2.3. Characterization of synthesized nano heterojunction photocatalyst

(i) UV-vis spectroscopy: Optical characterization was conducted with UV-vis spectroscopy (Perkin Elmer, LAMBDA750) and Tauc's relationship was used to calculate the heterojunction photocatalyst's band gap. (ii) X-ray diffraction (XRD): Structural characteristics and phase shifts of Cu-N:ZnO/TiO_2 heterojunction photocatalysts were analyzed by XRD (PANalytical, EMPYREAN, X-Ray Lab, IITB) with Cu Kα radiation (λ = 1.54184 Å). (iii) Field emission scanning electron microscopy (FE-SEM): The surface morphology of Cu-

10.57647/ijc.2026.1602.15

N:ZnO/TiO_2 photocatalysts was analyzed using FE-SEM (JEOL JSM-7600F, SAIF, IITB). (iv) Energy Dispersive X-ray Spectroscopy (EDS): Elemental analysis and mapping of the co-doped photocatalysts were conducted using energy-dispersive EDS mapping (Apreo 2S Highvac, Thermofisher Scientific, Accuphychem Analytics). (v) X-ray Photoelectron Spectroscopy (XPS): chemical composition, oxidation states, and electronic structure of synthesized Cu-N:ZnO/TiO_2 photocatalyst were analysed by XPS analysis (ESCA+ Omicron Nanotechnology, Germany, Accuphychem Analytics).

3. Result and discussion

3.1. UV–Visible Diffuse Reflectance Spectroscopy (DRS) Analysis

The optical properties of the Cu-N co-doped ZnO/TiO_2 heterojunction photocatalysts were evaluated using UV-Visible diffuse reflectance spectroscopy (UV-Vis DRS) in the wavelength range of 250-650 nm. The absorbance spectra revealed a noticeable red shift in the absorption edge of the modified samples compared to pristine TiO_2, indicating enhanced visible light harvesting ability. To quantitatively estimate the optical band gap energy (Eg), the diffuse reflectance data (R) were converted to the Kubelka–Munk function F(R) using the relation [22,23]:

$$F(R_\infty) = \frac{(1-R_\infty)^2}{2R_\infty} \quad (1)$$

where R_∞ is the reflectance of an optically thick sample. Under the Kubelka-Munk theory, F(R) is proportional to the absorption coefficient (α) assuming constant scattering across wavelengths. This relationship allows the optical band gap to be evaluated using the Tauc relation [23,24].

$$[F(R)\,h\nu]^{1/n} = k(h\nu - Eg) \quad (2)$$

Here, n = ½ corresponds to the optical direct allowed transition, $h\nu$ is the photon energy (eV), α is the linear absorption coefficient of the material, k is model adjustment constant, and Eg is the optical band gap (eV). Tauc's plot, as shown in Fig. 2, was used to estimate the direct band gap (Eg) of the synthesized photocatalysts. Among all synthesized photocatalysts, the optimal 7% Cu-N(3%):ZnO/TiO_2 heterojunction exhibited the lowest band gap of 2.97 eV, compared to 3.19 eV for pure TiO_2 [21], suggesting a substantial narrowing of the energy gap. This red shift is attributed to the synergistic effect of Cu and N co-doping, which introduces impurity energy levels near the conduction and valence bands, thereby facilitating visible light excitation. The reduced band gap enables broader solar spectrum absorption, improving charge separation and photocatalytic activity under visible light irradiation. Hence, the Cu-N co-doped ZnO/TiO_2 heterostructure presents promising potential for efficient photocatalytic degradation of organic pollutants in wastewater under solar illumination.

3.2. X-ray diffraction (XRD)

Structural characteristics of the developed heterojunction photocatalysts were further investigated using XRD. The XRD data were collected within a 2θ range of 10° to 80°. Fig. 3 exhibits distinct and sharp diffraction peaks, confirming the highly crystalline nature of the material.

Fig. 3 shows major diffraction peaks at 2θ values of approximately 25.3°, 36.9°, 37.8°, 48°, 53.9°, 55°, and 62.7°, corresponding to the (101), (103), (004), (200), (105), (211), and (204) lattice planes of anatase TiO_2, respectively, in accordance with JCPDS file No. 21-1272 [25]. Similarly, ZnO peaks located at 35.10°, 47.81°, and 62.60° matches with (100), (002), and (102) planes, respectively, as per JCPDS file No. 036-1451 [16]. Based on the patterns, TiO_2 is confirmed to have a crystalline anatase structure, while ZnO is confirmed to have a hexagonal wurtzite structure [26].

This confirms the successful formation of a composite material consisting of both TiO_2 and ZnO phases. In addition, a weak diffraction feature observed near 2θ ≈ 43.07° may be associated with copper-related species corresponding to the (111) plane, according to JCPDS file No. 00-05-0667 and No. 00-48-1548 [27,28]. However, due to the low Cu loading and the non-plasmonic nature of the system, the presence of bulk metallic Cu is unlikely. Similar diffraction features in Cu-doped ZnO/TiO_2 [21], systems have been attributed to highly dispersed CuO/Cu_2O phases or to lattice distortion induced by Cu incorporation rather than crystalline Cu° formation [29]. This interpretation is further supported by XPS analysis, which confirms the predominance of Cu^{2+} species, indicating that copper is mainly incorporated into the oxide lattice or exists in an oxidized state rather than as metallic Cu. This suggests that the copper ions were successfully incorporated into the lattice structure of either TiO_2 or ZnO. As reported in several studies, nitrogen doping does not generate new XRD peaks in either ZnO or TiO_2 rather, it causes subtle shifts in existing ZnO (e.g., (100), (002), (101)) and TiO_2 (e.g., (101), (200)) reflections, along with slight broadening or reduced intensity, this is due to the substitutional addition of N into oxygen sites and the resulting lattice distortion and strain [30,31]. These results confirm the successful formation of 7% Cu-N(3%):ZnO/TiO_2 heterojunction composites as well as the incorporation of copper and nitrogen onto the ZnO/TiO_2 heterojunction. The Debye-Scherrer equation (Equ. 3) was utilized to estimate the crystallite sizes of all the photocatalysts that were synthesized, which is commonly employed to calculate the crystal size of nanoparticles [32,33].

10.57647/ijc.2026.1602.17

$$D = \frac{K\lambda}{\beta * Cos\theta} \quad (3)$$

Here, θ is the Bragg diffraction angle (in radians), D represents the average crystallite size, K is the Scherrer constant (typically 0.9), β is the full width at half maximum (FWHM) of the diffraction peak (in radians), and λ is the wavelength of the incident X-ray. Based on the XRD analysis, average crystallite size decreased from 36.08 nm for 7% Cu-doped ZnO/TiO_2 to 28.35 nm for 7% Cu-N(3%):ZnO/TiO_2. The smaller crystallite size can be attributed to the incorporation of nitrogen atoms into the crystal lattice, which induces lattice distortions and hinders crystal growth during synthesis. Co-doping with non-metal elements like nitrogen introduces additional defects and strain, which restricts particle coalescence and promotes smaller grain formation. A smaller crystallite size typically leads to enhanced photocatalytic activity because of the resulting increase in surface area and more active sites for photoreactions. So, the decrease in crystal size that happens with nitrogen co-doping is seen as a good thing for boosting the photocatalytic performance of the heterojunction material [30,34,35]. Although the Williamson–Hall method can separate size- and strain-induced broadening, the Debye–Scherrer approach was adopted here to reliably compare relative crystallite size evolution among the synthesized photocatalysts, as similarly reported in recent heterojunction studies [36].

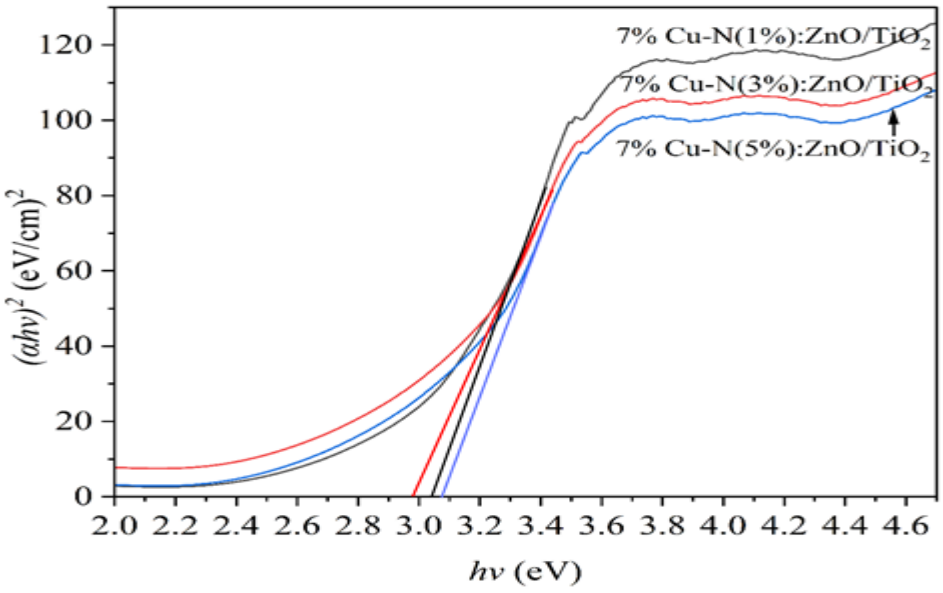

Figure 2. Tauc's plot of 7% Cu-N:ZnO/TiO_2 (1wt%-5wt% N co-doped) heterojunction photocatalyst

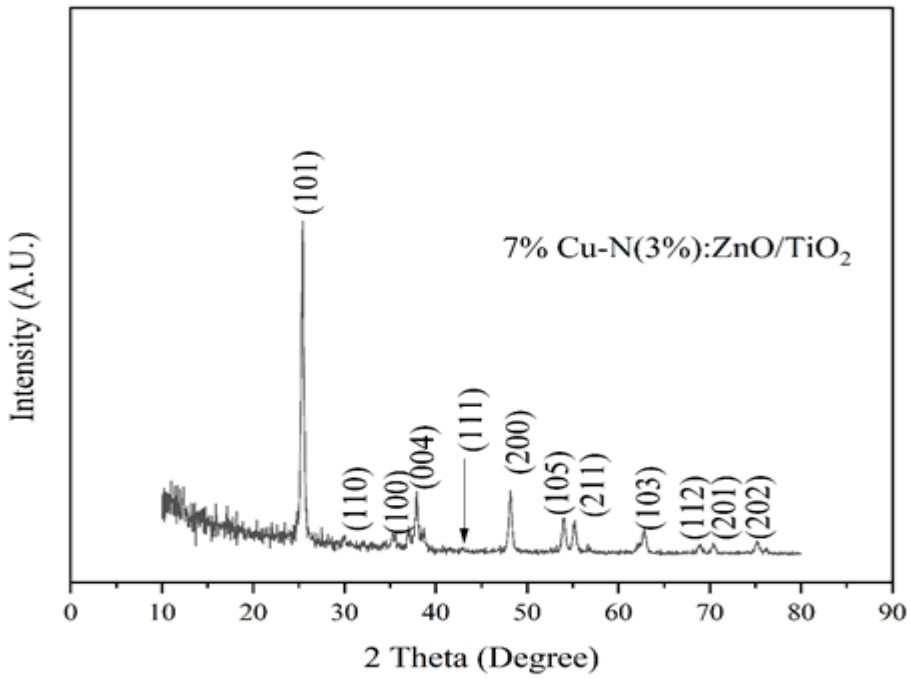

Figure 3. XRD plot of synthesized 7% Cu-N(3%):ZnO/TiO_2 heterojunction photocatalyst

10.57647/ijc.2026.1602.15

3.3. Field emission scanning electron microscopy (FE-SEM) and Energy Dispersive X-ray Spectroscopy (EDS)

Fig. 4(a and b) shows the surface morphology of the optimized 7% Cu-N(3%):ZnO/TiO_2 heterojunction photocatalyst materials was examined using FE-SEM which confirmed the almost spherical shape of the synthesized catalyst and product with uniform size distribution [37]. Furthermore, it was reported that co-doping photocatalytic materials with copper and nitrogen significantly improves their physical structure. For instance, copper and nitrogen as a dopant can enhances surface morphology, reduced crystalline size and atomic arrangement of photocatalyst [38–40]. Therefore maximum photodegradation efficiency observed in 7% Cu-N(3%):ZnO/TiO_2 among prepared photocatalyst. Fig. 5 confirms homogeneous distribution of Cu, Zn, Ti, O, and N elements within the in 7% Cu-N(3%):ZnO/TiO_2 heterojunction. The Cu (6.6 wt%) and N (2.6 wt%) contents are close to their nominal doping levels, confirming successful incorporation.

Furthermore, Fig. 6(a-d) shows the elemental distribution mapping, which uses colored dots to represent the elements, confirmed the presence of Cu, N, O, Ti, and Zn in the photocatalyst. The 7% Cu-N(3%):ZnO/TiO_2 catalyst looks to be homogenous based on the EDS mapping [24].

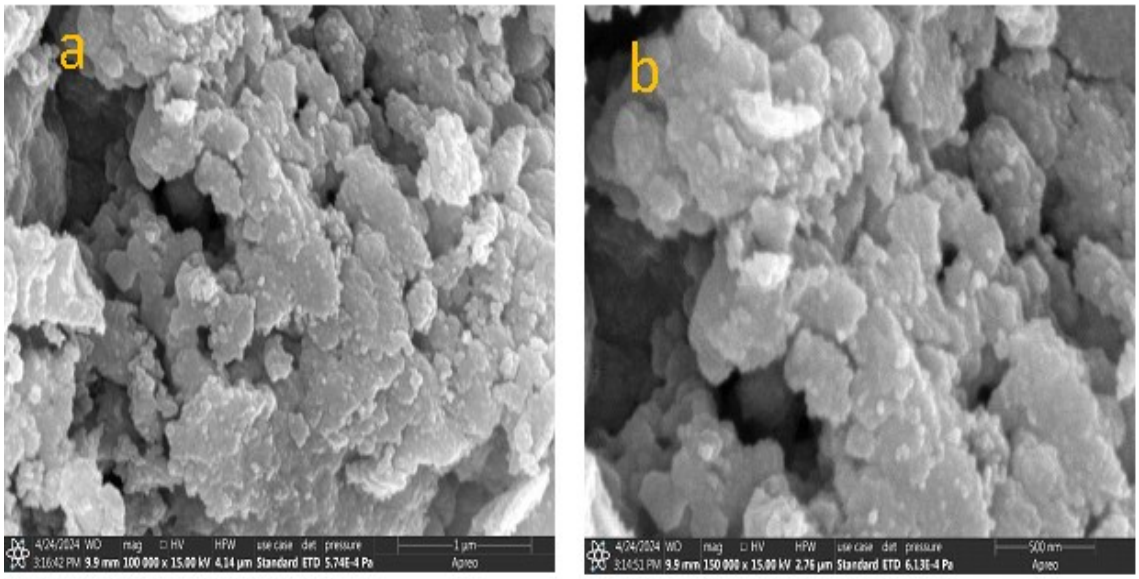

Figure 4. (a and b) FE-SEM of synthesized 7% Cu-N(3%):ZnO/TiO_2 heterojunction photocatalyst

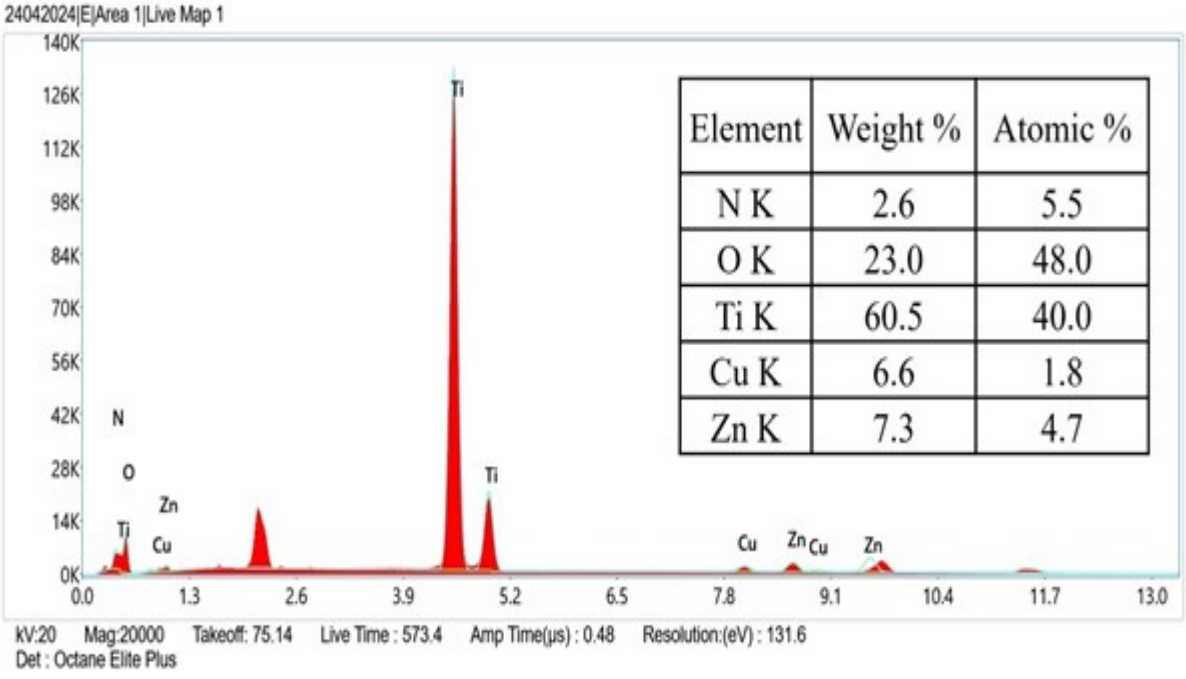

Element	Weight %	Atomic %
N K	2.6	5.5
O K	23.0	48.0
Ti K	60.5	40.0
Cu K	6.6	1.8
Zn K	7.3	4.7

Figure 4. EDS of synthesized 7% Cu-N(3%):ZnO/TiO_2 heterojunction photocatalyst

10.57647/ijc.2026.1602.17

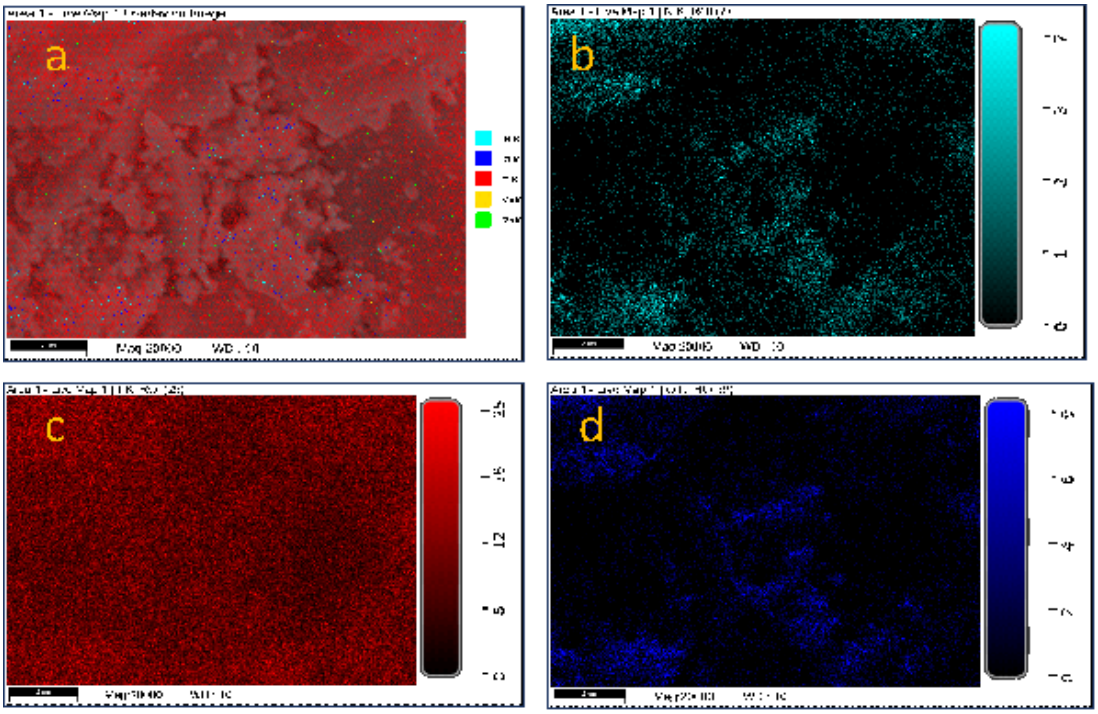

Figure 5. EDS Elemental mapping (a-d) of 7% Cu-N(3%):ZnO/TiO_2 heterojunction photocatalyst

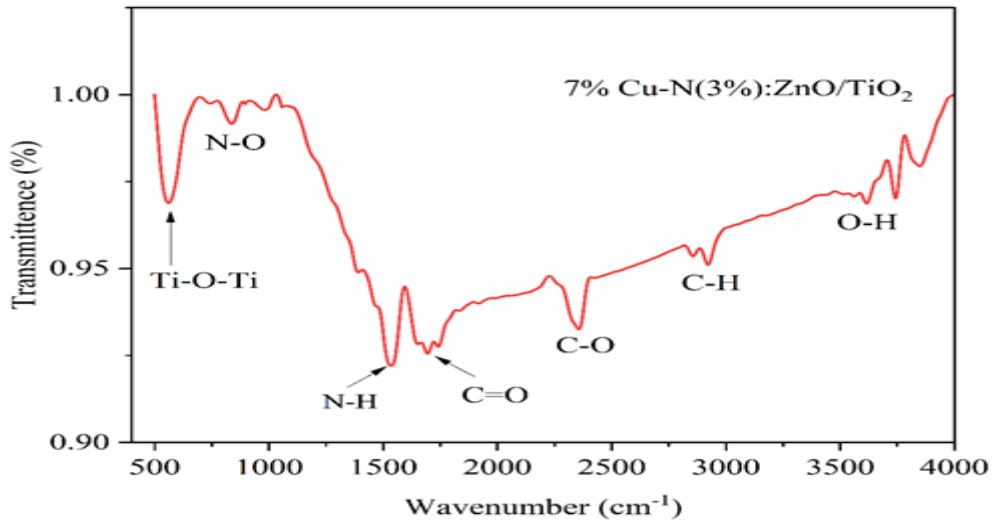

Figure 6. FTIR of synthesized 7% Cu-N(3%):ZnO/TiO_2 heterojunction photocatalyst

3.4. X-ray Photoelectron Spectroscopy (XPS)

Fig. 8 presents the XPS investigation of the photocatalyst, illustrating its elemental composition and surface chemical states. The survey spectrum Fig. 8(a) clearly identifies Ti, Zn, O, Cu, N, and C as the constituent elements of the material. In Fig. 8(b), two distinct signals at 458.16 eV and 464.07 eV are observed, which can be assigned to the Ti $2p_{3/2}$ and Ti $2p_{1/2}$ levels, respectively, confirming the presence of Ti^{4+} in the TiO_2 lattice [42,45]. Fig. 8(c) displays two characteristic peaks at 1020.92 eV and 1044.08 eV, assigned to Zn $2p_{3/2}$ and Zn $2p_{1/2}$, respectively, which verify the presence of Zn^{2+} species in the photocatalyst [46,47]. Copper is evidenced by Cu 2p peaks at 951.68 eV and 931.6 eV in the Cu 2p spectrum can be attributed to Cu^{2+} 2p1/2 and Cu^{2+} 2p3/2, respectively shown in Fig. 8(d) [48]. Nitrogen is detected in the N 1s at 397.6 eV. binding near 396-397 eV is often attributed to substitutional N (Ti-N or O-Ti-N), whereas components near 399-401 eV are commonly linked to interstitial N or surface N-species shown in Fig. 8(e) [49,50].

Oxygen shows a strong O 1s envelope at 529.43 eV, typically comprising lattice O_2 with higher binding energy shoulders from surface -OH/defect oxygen shown in Fig. 8(f). A C 1s peak at 284.8 eV arises from ubiquitous hydrocarbon contamination and is frequently used for charge referencing shown in Fig. 8(g) [51]. Overall, these confirmed a 7% Cu-N(3%):ZnO/TiO_2 surface with oxidized Ti^{4+}/Zn^{2+} lattices.

10.57647/ijc.2026.1602.17

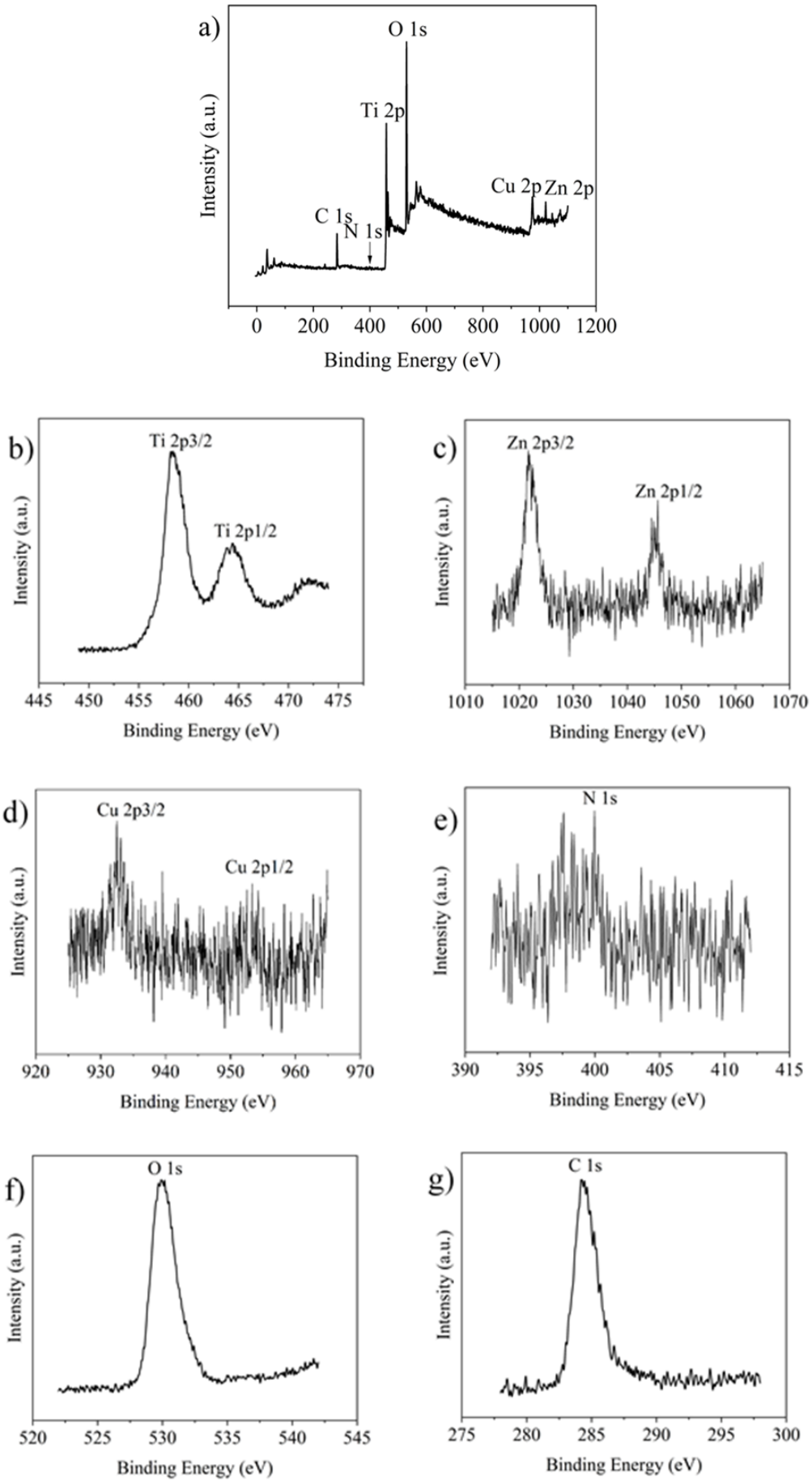

Figure 7. XPS analysis of 7% Cu-N(3%):ZnO/TiO_2 heterojunction photocatalyst a) Survey b) Ti 2p peak c) Zn 2p peak d) Cu 2p e) N 1s peak f) O1s peak g) C1s peak

10.57647/ijc.2026.1602.17

3.5. Possible Photocatalystic degradation mechanism for 7%Cu-N(3%):ZnO/TiO_2

The 7% Cu–N(3%):ZnO/TiO_2 photocatalyst exhibits enhanced visible-light activity due to N induced mid-gap states and Cu redox centres. The conduction band (CB) edge (E_{CB}) and valence band (VB) edge (E_{VB}) potential of ZnO and TiO_2 can be determined using the Mulliken electronegativity equation as follows [52,53]:

$$E_{CB} = \chi - E_e - 0.5\ E_g \quad (4)$$

$$E_{VB} = E_{CB} + E_g \quad (5)$$

Where, E_e represents energy of free electrons on the hydrogen scale (E_e = 4.5 eV), χ represents the electronegativity of the semiconductor and E_g refers to the band gap energy of the semiconductor. For ZnO, TiO_2 and 7% Cu-N(3%):ZnO/TiO_2, χ is 5.79 eV, 5.81 eV and 5.81 eV respectively. E_g for ZnO, TiO_2 and 7% Cu-N(3%):ZnO/TiO_2 is 3.3 eV, 3.19 eV and 2.97 eV respectively. Mulliken electronegativity analysis places the band edges at E_{CB}(ZnO) = -0.36 eV, E_{VB}(ZnO) = +2.94 eV; E_{CB}(TiO_2) = -0.29 eV, E_{VB}(TiO_2) = +2.90 eV; and for the 7% Cu–N(3%):ZnO/TiO_2 nanoheterojunction E_{CB} = -0.18 eV, E_{VB} = +2.80 eV. These relative positions indicate a Type-II (staggered) heterojunction in which photogenerated electrons preferentially transfer from ZnO CB to TiO_2 CB while holes migrate from TiO_2 VB to ZnO VB, promoting spatial charge separation and suppressing recombination [54,55]. Co-doping modifies this picture [12,56]: substitutional N introduces N 2p mid-gap states above the O 2p valence band, narrowing the effective band gap and enhancing visible-light absorption and hole localization, whereas Cu^{2+}/Cu^{+} sites act as reversible electron traps and mediators that facilitate reduction of dissolved O_2 to $^{\bullet}O_2^-$ ($Cu^{+} + O_2 \rightarrow Cu^{2+} + {}^{\bullet}O_2^-$) even though the heterojunction CB is only marginally negative relative to the $O_2/{}^{\bullet}O_2^-$ potential shows in Fig. 9. As a result, the photocatalytic degradation of TBG proceeds via hole and •OH-driven oxidation (E_{VB} = +2.80 eV > +2.38 eV vs NHE) together with Cu assisted superoxide pathways, leading to stepwise hydroxylation, dealkylation, chromophore cleavage and eventual mineralization- the combined effect being a Type-II heterojunction with Cu/N-mediated (modified Type-II heterojunction) enhancements that impart some of the activity advantages of Z-scheme systems. Therefore, although the charge transfer pathway is not a classical Z-scheme, the Cu/N-mediated modified Type-II heterojunction preserves strong redox ability while ensuring efficient charge separation, in agreement with recent reports on step-scheme-like heterostructures [17,57]. This charge transfer pathway schematically illustrated in the proposed mechanism, effectively suppresses electron-hole recombination and accelerates dye degradation, which is consistent with the observed band gap reduction, enhanced degradation efficiency, and significant COD removal. The following reactions demonstrate the reactions taking place at the conduction band of photocatalyst:

$$\text{Photocatalyst (Cu-N:ZnO/TiO}_2\text{)} + h\nu \rightarrow \text{Photocatalyst } (e^-_{CB} + h^+_{VB}) \quad (6)$$

$$e^-_{CB} + O_2 \rightarrow O_2^{\bullet-} \quad (7)$$

$$h^+_{VB} + H_2O \rightarrow OH^{\bullet} \quad (8)$$

$$\text{TBG} + h^+_{VB} / OH^{\bullet} / O_2^{\bullet-} \rightarrow \text{Degraded Product} + CO_2 + H_2O \quad (9)$$

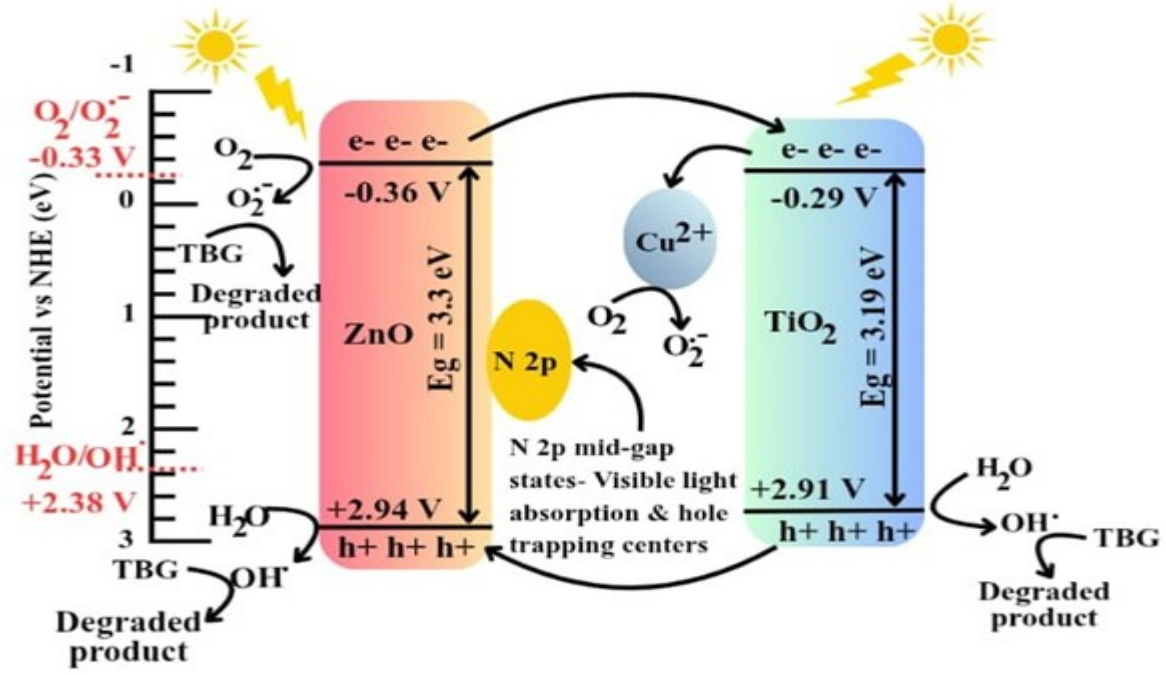

Figure 9. Schematic energy band alignment of the 7%Cu-N(3%):ZnO/TiO_2 modified Type-II heterojunction photocatalyst with band edge positions referenced to the normal hydrogen electrode (NHE)

10.57647/ijc.2026.1602.17

3.6. Photocatalytic degradation study of turquoise blue G (TBG) dye

Photocatalytic degradation experiments were carried out in a slurry-type photoreactor, where the photocatalyst was uniformly suspended in the wastewater under continuous magnetic stirring and irradiated using a 150 W medium-pressure mercury vapor lamp (MPMVL); the detailed reactor configuration and schematic diagram have been reported in our previously published work [21]. Fig. 10 (a) gives the photocatalytic degradation profiles of 1 liter of 20 ppm TBG dye using 0.5 g weight of all synthesized 7% Cu-N:ZnO/TiO_2 heterojunction photocatalyst. In the presence of UV light, 7% Cu-N(3%):ZnO/TiO_2 showed significant enhancement, achieving a C/C_0 value of approximately 0.02 after 2.5h. This performance was 1.57 times greater than pure TiO_2 [21].

This indicates that 7% Cu-N(3%):ZnO/TiO_2 effectively enhances the photoactivity compared to pure TiO_2 alone. Specifically, the 7% Cu-N(3%):ZnO/TiO_2 formulation consistently displayed lower C/C_0 values across various reaction durations, indicating superior degradation performance. Notably, 7% Cu-N(3%):ZnO/TiO_2 demonstrated the highest degradation efficiency of 98.07% among all synthesized photocatalysts [21]. Preliminary dark adsorption and photolysis tests showed negligible TBG removal, confirming that dye degradation occurs predominantly via photocatalytic processes. The photocatalytic degradation kinetics of Turquoise Blue G (TBG) were analyzed using the Langmuir-Hinshelwood model. As the initial dye concentration was (20 ppm), the reaction followed a pseudo-first-order kinetic model, expressed by the equation $\ln Co/Ct = kapp * t$. where k_{app} is the apparent rate constant [58,59].

As illustrated in Fig. 10 (b), the linear plots of lnC_0/C_t versus irradiation time show a strong correlation, with all R^2 values exceeding 0.991. Table 1 shows kinetic parameters of synthesized photocatalyst. The 7% Cu-N(3%):ZnO/TiO_2 heterojunction exhibited the highest photocatalytic activity, with a k_{app} of 1.6347 h^{-1} (0.0272 ± 0.002 min^{-1}). This rate is approximately 1.38 times and 1.27 times higher than the 1% and 5% nitrogen-doped variants, respectively.

The superior kinetic performance of the 3% N-doped sample is attributed to the optimal concentration of nitrogen-induced mid-gap states and copper redox centers, which maximize visible-light absorption while minimizing the recombination of photogenerated charge carriers. Higher doping levels (5% N) likely introduced excessive recombination centers, leading to the observed decrease in k_{app}. Table 2 compares the photocatalytic performance of the present 7% Cu-N(3%):ZnO/TiO_2 nanoheterojunction with recently reported heterojunction photocatalysts for organic dye degradation. As shown in the comparison, the present photocatalyst achieved a high degradation efficiency of 98.07% for Turquoise Blue G (TBG) within 150 min, accompanied by an apparent rate constant (k_{app} = 0.0272 min^{-1}), which is among the highest values reported for UV-driven heterojunction systems. Furthermore, the degradation efficiency achieved in this work is comparable or superior to other visible-light-active heterojunctions targeting common dyes such as Rhodamine B, Methylene Blue, and Congo Red, despite focusing on the more structurally complex TBG dye, for which very limited literature reports exist.

The results demonstrate that the co-doped Cu-N:ZnO/TiO_2 system shows competitive or superior degradation efficiency and favorable band gap narrowing compared to other state-of-the-art heterostructures reported in the literature under UV, visible and solar irradiation. Fig. 11 illustrates the nearly clean water that was obtained after 150 minutes of photocatalytic treatment with 7% Cu-N(3%):ZnO/TiO_2. The photodegradation efficiency is determined using the following formula:

$$Photodegradation\ efficiency\ (\%) = \frac{Intial\ Concentration - Final\ Concentration}{Intial\ Concentration} x100 \quad (10)$$

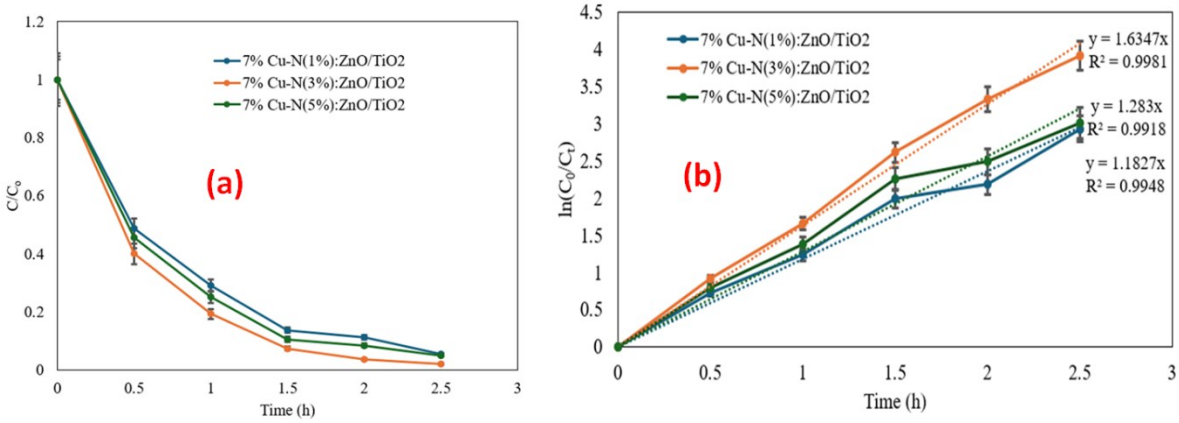

Figure 10. (a). Photocatalytic degradation of TBG dye using different 7% Cu-N:ZnO/TiO_2 varied nitrogen dopant (1%, 3% & 5%) (b). Reaction kinetic study for the degradation of TBG dye by the synthesized photocatalyst

10.57647/ijc.2026.1602.17

Table 1. Kinetic parameters of all synthesized photocatalyst

Photocatalyst Sample	k_{app} (h^{-1})	k_{app} (min^{-1})	R^2	Degradation Efficiency (%) (150 min)	Remarks
Pure TiO_2	0.4452	0.0074	0.9525	62.36	Mentioned in previously published research work [21]
ZnO/TiO_2	0.8475	0.0141	0.9708	85.07	
3% Cu:ZnO/TiO_2	0.8475	0.0141	0.9708	86.22	
5% Cu:ZnO/TiO_2	0.9523	0.0158	0.9773	90.96	
7% Cu:ZnO/TiO_2	1.2806	0.0163	0.9795	95	
9% Cu:ZnO/TiO_2	0.8507	0.0141	0.9713	84.36	
7% Cu-N(1%):ZnO/TiO_2	1.1827	0.0197	0.9948	94.65	Present Work
7% Cu-N(3%):ZnO/TiO_2	1.6347	0.0272	0.9981	98.07	
7% Cu-N(5%):ZnO/TiO_2	1.283	0.0214	0.9918	95.04	

Table 2. Comparison of Recent Heterojunction Photocatalysts for Dye Degradation

Photocatalyst	Target pollutant	Synthesis Method	Light source	Band gap (eV)	Degradation efficiency (%)	Time (min)	k_{app} (min^{-1})	Stability / cycles	Ref.
7% Cu-N(3%): ZnO/TiO_2	Turquoise Blue G	RTSG	UV (150 W MPMVL)	2.97	98.07	150	0.0272 (highest in study)	Base heterojunction 84.3% degradation efficiency retention	Present work
Cu-ZnO/TiO_2 Z-scheme	Congo Red	Sonochemical	Sunlight	2.68	98	20	0.094	-	[60]
g-C_3N_4/BiOI p-n heterojunction (2D/2D)	Rhodamine B (RhB)	Simple precipitation and a high temperature calcination	Simulated sunlight	-	99.7	60	0.087	After 5 cycles, degradation efficiency decreasing by only 1.2%.	[61]
ZnO-TiO_2 n-n heterojunction	Tetracycline	-	Visible	3.1	97	60	0.0675	Reported stable efficiency	[62]
ZnO-[10%]WO_3 and ZnO-[10%]BiOI heterostructure	Methyl Orange	ZnO- Sol gel method	Visible	3.16 (10% WO_3) and 3.0 (10% BiOI)	100 (10% WO_3 and 10% BiOI)	90 (10% WO_3) and 120 (10% BOI)	0.05(10 % WO_3) and 0.04 (10% BiOI)	-	[63]
g-C_3N_4/ZnO-W/Co_x heterojunction	Methylene Blue	Coprecipitation method	Visible	2.28 -3.22	90	90	0.037	After 5 cycles, degradation efficiency 82%	[64]
$ZnMn_2O_4/TiO_2$ heterojunction	Methylene Blue	Sol-gel autocombustion	Solar	1.97	99	180	0.02644	After 5 cycles, efficiency decreased slightly by 10 % for $ZnMn_2O_4$ and 8 % for the p-$ZnMn_2O_4$/n-TiO_2 heterojunction.	[65]

10.57647/ijc.2026.1602.17

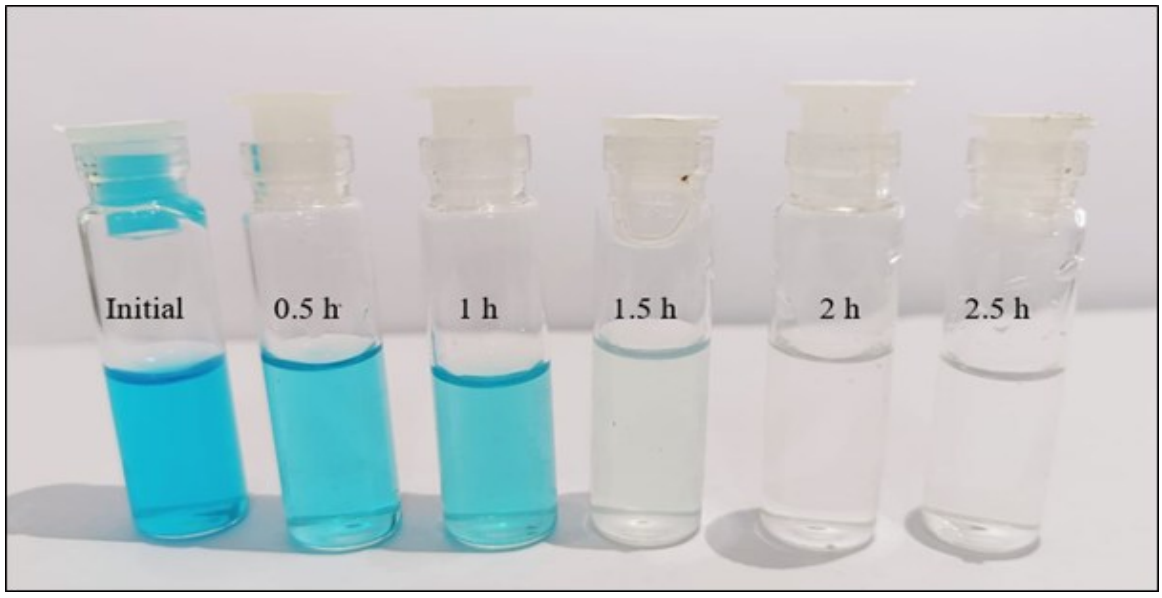

Figure 11. Photocatalytic degradation condition of TBG dye was assessed using 7% Cu-N(3%):ZnO/TiO_2 after every 0.5h

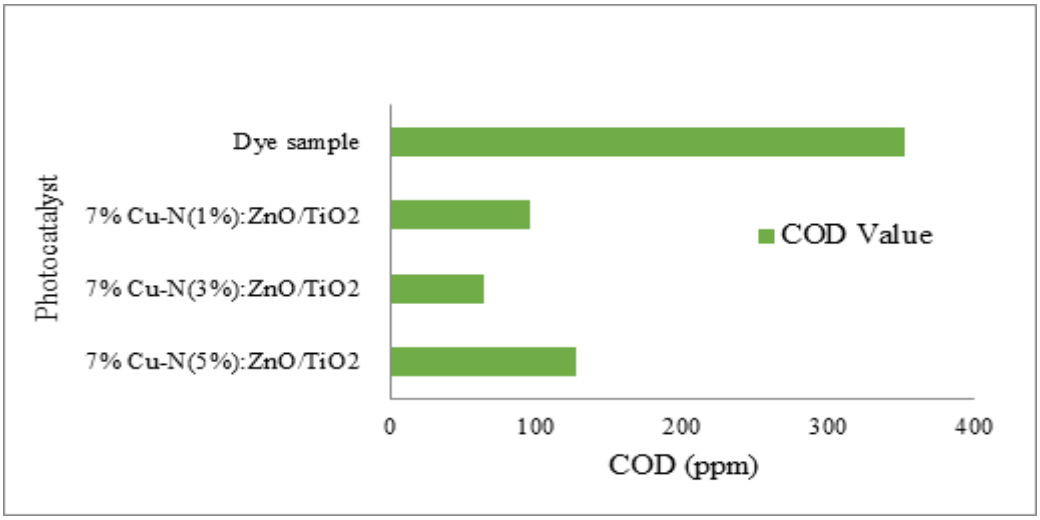

Figure 12. COD of TBG dye waste water treated by 7% Cu-N:ZnO/TiO_2 (N = 1wt% to 5wt%) synthesized photocatalyst

3.6.1. *Chemical Oxygen Demand (COD) Measurement*

One common technique for determining the amount of organic matter in waste water is the COD treatment method. The COD of the TBG dye waste water was estimated initially and after the photocatalytic treatment. COD of dye waste water treated by synthesized 7% Cu-N:ZnO/TiO_2 (1wt% - 5wt% N dopant amount). The decrease in COD values of the dye solution after treatment suggests that the dye molecules have undergone degradation. Fig. 12 showed among all synthesized photocatalyst, 7% Cu-N(3%):ZnO/TiO_2 maximum 81.82% COD degradation efficiency was obtained which is 5.5 times reduced from initial COD of TBG waste water. The COD degradation efficiency is calculated from following equation.

$$COD\ degradation\ efficiency\ (\%) = \frac{Intial\ COD - Final\ COD}{Intial\ COD} x100 \quad (11)$$

3.7. Design of Experiment (DoE) by RSM along with CCD

Optimization of solar photocatalytic degradation efficiency of the synthesized co-doped 7% Cu-N:ZnO/TiO_2 heterojunction photocatalyst was conducted using RSM study along with CCD. Two independent process variables were selected:
(i) co-dopant Nitrogen doping amount (1wt% - 5wt%) and (ii) degradation time (1.5 - 2.5 h), while the response variable was the photocatalytic degradation efficiency (%) of TBG dye wastewater measured under UV light mentioned in Table 3. The CCD was used to plan the experimental runs by incorporating factorial, axial, and center points. This design allowed for the evaluation of linear and quadratic effects, along with the interactions among the variables. The experimental data of CCD were fitted using a second-order (quadratic) polynomial equation as follows[5,19]:

$$Y\ (\%) = a_0 + a_2x_1 + a_2x_2 + a_{12}x_1x_2 + a_{11}x_1^2 + a_{22}x_2^2 \quad (12)$$

where Y means the response variable (Photodegradation efficiency), a_i, a_{ii}, and a_{ij} denotes regression coefficients corresponding to linear terms, quadratic terms and interaction effects respectively. The variables x_i indicate the independent parameters under investigation.

3.7.1. *Statistical Analysis and Model Development*

The experimental run with corresponding responses for the degradation of TBG dye, as suggested by the CCD design, are presented in Table 4. Based on this design, the empirical relationship between the independent variables and the response was described by a second-order polynomial equation expressed in terms of actual factors.

Photodegradation efficiency (%) = 49.7825 + 7.82354 Nitrogen doping amount + 27.34415 Dye Degradation Time - 0.845 Nitrogen doping amount × Dye Degradation Time - 0.963982 Nitrogen doping amount² - 4.55366 Dye Degradation Time²

The adequacy of the model was assessed using analysis of variance (ANOVA). According to the ANOVA results of the empirical second-order polynomial model presented in Table 5, the model exhibits a high F-value of 179.61, confirming its strong statistical significance [66].

The probability that the model's F-value occurred due to random noise is only 0.01%. The model's p-value of <0.0001 further confirms its statistical significance [5]. The lack-of-fit value of 3.54 indicates that the lack of fit is insignificant when compared to the pure error. There is a 12.68% chance that the lack-of-fit F value could occur due to noise. The non-significant lack of fit confirms the good predictability of the model.

The pred R-squared of 0.9567 is in reasonable agreement with the adj R-squared of 0.9867, confirming good predictability of the model [67]. The accuracy of the model is illustrated in Fig. 13, which compares the measured values against the predicted responses of the model for the degradation of TBG dye.

As per ANOVA study, x_1, x_2, x_1x_2, x_1^2 and x_2^2 are significant model terms.

All independent variables, their interactions, and second order terms exhibited high statistical significance with p-values < 0.001 [66,67]. *P-values* below 0.05 confirm that the corresponding model terms are statistically significant [68].

Table 3. Range and levels of the independent experimental variables

Factor	Range and Levels		
	-1	0	+1
x_1-Nitrogen doping amount (wt%)	1	3	5
x_2-Dye Degradation Time (h)	1.5	2	2.5

Table 4. Experimental matrix of independent parameters and response

		Factor-1	Factor-2	Response
Std Order	Run Order	x_1-Nitrogen doping amount (wt%)	x_2-Dye Degradation Time (h)	Y-Photodegradation efficiency (%)
12	1	3	2	95.633
8	2	3	2.7071	98
9	3	3	2	95.83
13	4	3	2	95.8
3	5	1	2.5	94.65
2	6	5	1.5	89.71
7	7	3	1.29289	88.71
4	8	5	2.5	94.64
6	9	5.82843	2	88.71
5	10	0.171573	2	87.13
11	11	3	2	96.22
10	12	3	2	96.42
1	13	1	1.5	86.34

Table 5. ANOVA Results for the Response Surface Quadratic Model

Source	Sum of Squares	df	Mean Square	F-value	p-value	
Model	200.03	5	40.01	179.61	< 0.0001	significant
x_1-Nitrogen doping amount (%)	2.84	1	2.84	12.73	0.0091	
x_2-Dye Degradation Time (h)	8.91	1	8.91	39.98	0.0004	
x_1 x_2	2.86	1	2.86	12.82	0.0090	
x_1^2	103.43	1	103.43	464.37	< 0.0001	
x_2^2	9.02	1	9.02	40.48	0.0004	
Residual	1.56	7	0.2227	-	-	
Lack of Fit	1.13	3	0.3775	3.54	0.1268	not significant
Pure Error	0.4265	4	0.1066	-	-	
Cor Total	201.59	12	-	-	-	

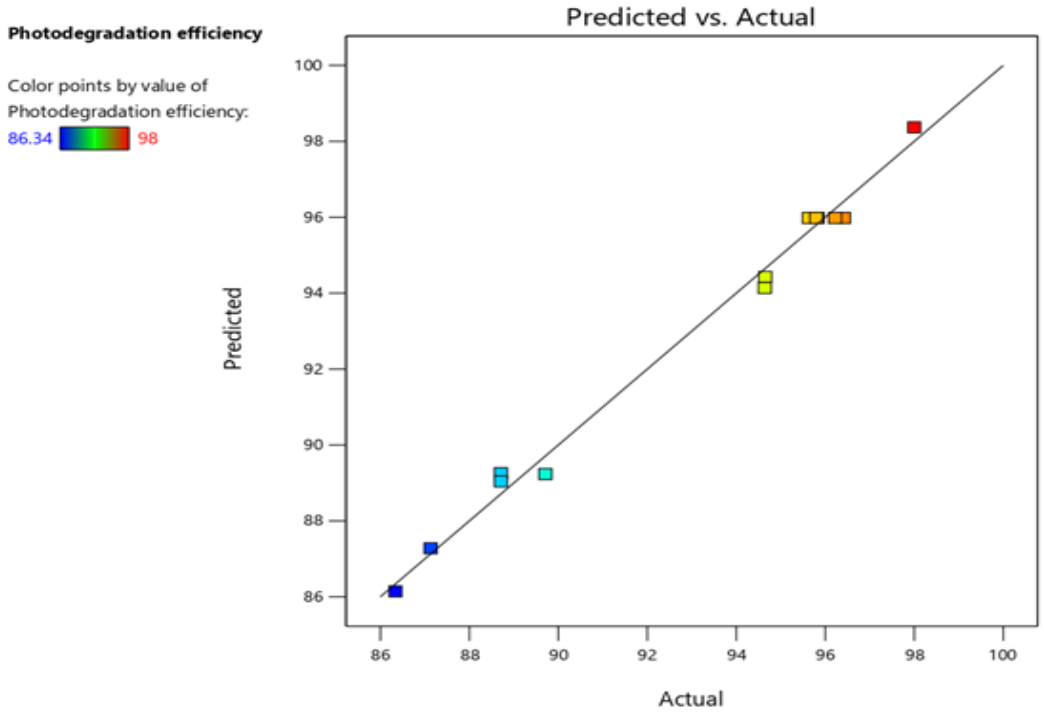

Figure 13. Accuracy plot comparing the measured values with the predicted responses for TBG dye degradation

3.7.2. *Effects of the Factors and Their Interaction on the Responses*

The effects of process variables and their mutual interactions on photocatalytic performance were further elucidated through 3D response surface plots generated from the CCD-based regression model. These graphical surfaces are widely used in RSM studies to visualize the combined influence of two parameters and to pinpoint the optimum operating region. Fig. 14 illustrates that the interaction between catalyst load (nitrogen doping amount) and photodegradation time significantly influences the photocatalytic degradation efficiency. An increase in nitrogen content enhances the degradation efficiency until an optimal level is reached, beyond which additional doping produces only marginal improvement [69,70]. Likewise, extending the irradiation time steadily improves degradation efficiency [20,71,72]. These trends confirm that achieving maximum photocatalytic efficiency requires a balanced combination of optimal dopant loading and adequate reaction time. The synergistic interaction of these variables plays a decisive role in accelerating charge separation, enhancing visible-light absorption, and thereby promoting highly efficient TBG dye degradation.

3.7.3. *Optimization of interacting parameters on degradation efficiency*

Optimization of TBG dye degradation was carried out using the desirability function approach to identify the most favourable operating conditions. Numerical optimization tools were employed to locate the point that provides the highest overall desirability.

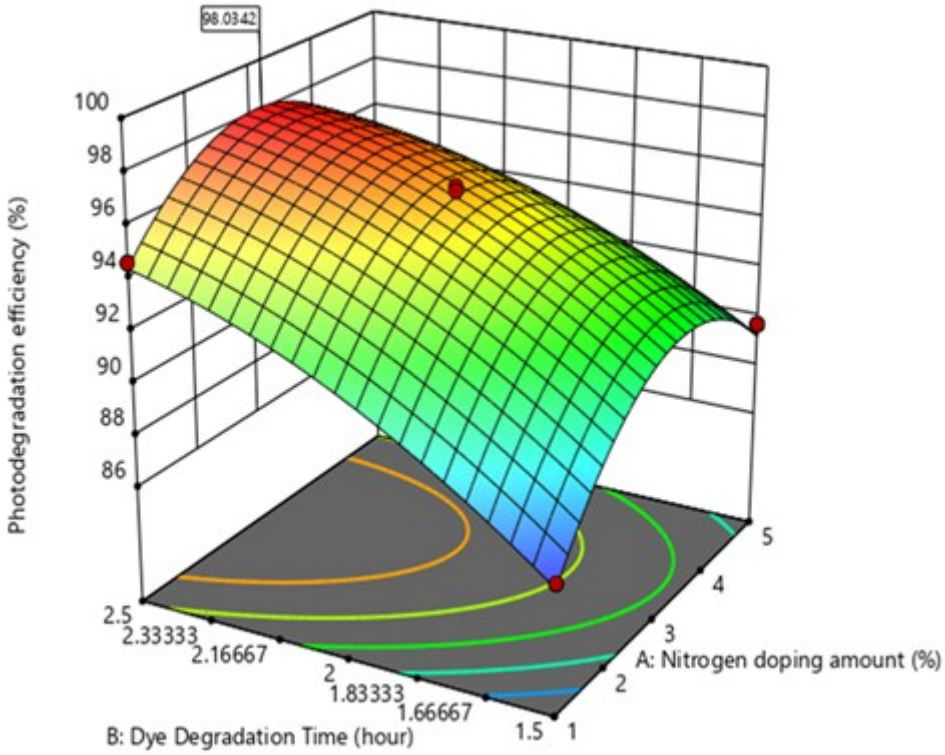

Figure 14. Effects of Nitrogen doping amount and dye degradation time on degradation efficiency of TBG Dye

Table 6. Limits, weight and importance of independent variables and response

Name	Goal	Lower Limit	Upper Limit	Lower Weight	Upper Weight	Importance
x_1:Nitrogen doping amount (%)	is in range	1	5	1	1	3
X_2:Dye Degradation Time (h)	is in range	1.5	2.5	1	1	3
Photodegradation efficiency (%)	maximize	86.34	98	1	1	5

Table 7. Predictive and experimental TBG dye degradation efficiency and optimum value of independent variables

Variables	Optimum Value	TBG dye Degradation efficiency (%)	
		Predictive efficiency (%)	Experimental efficiency (%)
x_1:Nitrogen doping amount (%)	2.887	98.123	98.07
x_2:Dye Degradation Time (h)	2.494		

The selected criteria and goal for each variable in relation to the degradation efficiency are summarized in Table 6. The importance level selected 5 to emphasize degradation efficiency which is the goal of this study. As per selection of upper and lower limits of independent parameters, lower and upper weight and importance level of response, the optimum conditions were found to be nitrogen doping amount (2.887 wt%), dye degradation time (2.494 h) to enhance TBG dye degradation efficiency 98.07%.

3.7.4. *Validation and confirmation of model*

A validation experiment was performed to assess the reliability of the model in estimating the highest degradation efficiency of TBG dye. From three successive experiments, an average maximum degradation efficiency of 98.07% was recorded which is in close agreement with the predictive efficiency 98.123%, as illustrated in Table 7.

The strong consistency observed between calculated and measured values validates the model's applicability for simulating the photocatalytic degradation of TBG dye.

4. Conclusion

A novel modified type-II heterojunction photocatalyst, 7% Cu-N:ZnO/TiO_2 (with nitrogen doping concentrations varying from 1 wt% to 5 wt%) was synthesized using a cost-effective sol-gel (RTSG) technique.

To investigate their optical behavior, crystal structure, morphology, surface chemistry, and bonding features, the

10.57647/ijc.2026.1602.17

synthesized photocatalysts were examined through UV–Vis, XRD, FE-SEM, XPS, and FTIR analyses. Optical studies showed that the 7% Cu-N(3%):ZnO/TiO_2 photocatalyst achieved the most significant band gap reduction (2.97 eV) compared to pure TiO_2 (3.19 eV). The reduction in band gap, confirmed by a red shift, enhances photocatalytic activity by enabling greater absorption of visible light from the solar spectrum.

Optimization and modelling of the process variables (nitrogen doping amount and dye degradation time) in the first time photocatalytic degradation of TBG dye using the novel 7% Cu-N(3%):ZnO/TiO_2 nano-heterojunction catalyst were carried out through Response Surface Methodology (RSM). The quadratic model described the relationship between the two independent variables and degradation efficiency of the TBG dye.

A good agreement was observed between model predictions and experimental measurements, confirming the predictive accuracy of the models at the 95% confidence level. At optimum condition, nitrogen doping amount (2.887 wt%), TBG dye degradation time (2.494 h), photocatalytic degradation efficiency achieved 98.07% which was 1.57 times higher than pure TiO_2 and reducing COD to a level 5.5 times lower than untreated wastewater.

The regression coefficient ($R^2 = 0.9923$) confirms an excellent agreement between the experimental data and the model predictions. From a practical perspective, the developed 7% Cu-N(3%):ZnO/TiO_2 photocatalyst offers significant potential for real-world wastewater treatment applications due to its low-cost synthesis via a room-temperature sol–gel route, high degradation efficiency, and substantial COD reduction.

The use of earth-abundant elements (Zn, Cu and N) and the demonstrated stability of the base heterojunction system make the material attractive for scalable slurry-type photocatalytic reactors commonly employed in industrial effluent treatment.

Moreover, the successful application of RSM-CCD for process optimization provides a valuable framework for translating laboratory-scale performance to pilot and full-scale treatment systems. These attributes highlight the feasibility of implementing the proposed photocatalyst for sustainable remediation of dye-contaminated industrial wastewater.

Acknowledgments

The authors acknowledge the Sophisticated Analytical Instrument Facility (SAIF), Indian Institute of Technology (IIT), Bombay, Mumbai, X-Ray Lab, Department of MEMS, Indian Institute of Technology (IIT), Bombay, Mumbai, Maharashtra, India, for rendering analytical services for this work.

Author's contributions
Authors have contributed equally in preparing and writing the manuscript.

Availability of data and materials
The data that support the findings of this study are available from the corresponding author, upon reasonable request.

Conflict of interest
The authors declare no conflict of interest.

Funding
This research did not receive any specific grant from funding agencies in the public, commercial or not-for-profit sectors.

References

[1] B. Yaou Balarabe, M.N. Illiassou Oumarou, A.S. Koroney, I. Adjama, A.R. Ibrahim Baraze, J. Nanotechnol. 2023 (2023) 1-12. https://doi.org/10.1155/2023/1292762

[2] S. Dutta, S. Adhikary, S. Bhattacharya, D. Roy, S. Chatterjee, A. Chakraborty, D. Banerjee, A. Ganguly, S. Nanda, P. Rajak, J. Environ. Manage. 353 (2024) 120103. https://doi.org/10.1016/j.jenvman.2024.120103

[3] Kusumlata, B. Ambade, A. Kumar, S. Gautam, Limnol. Rev. 24 (2024) 126–149. https://doi.org/10.3390/limnolrev24020007

[4] S. Sarkar, N.T. Ponce, A. Banerjee, R. Bandopadhyay, S. Rajendran, E. Lichtfouse, Environ. Chem. Lett. 18 (2020) 1569–1580. https://doi.org/10.1007/s10311-020-01021-w

[5] D. Titus, E.J.J. Samuel, J. Clust. Sci. 30 (2019) 1335–1345. https://doi.org/10.1007/s10876-019-01585-w

[6] D. Glažar, B. Simončič, Tekstilec. 66 (2023) 178–198. https://doi.org/10.14502/tekstilec.66.2023045

[7] M. Paiu, D. Lutic, L. Favier, M. Gavrilescu, Applied Sciences (Switzerland). 15 (2025) 5681. https://doi.org/10.3390/app15105681

[8] A.M. Sescu, L. Favier, D. Lutic, N. Soto-Donoso, G. Ciobanu, M. Harja, Water (Switzerland). 13 (2021) 19. https://doi.org/10.3390/w13010019

[9] B.J. Kim, J.H. Jeong, E.Y. Jung, T.Y. Kim, S. Park, J.A. Hong, K.M. Lee, W. Jeon, Y. Park, S.J. Kang, RSC Adv. 11 (2021) 12051–12057. https://doi.org/10.1039/d1ra00801c

[10] Y. Zhang, X. Bo, T. Zhu, W. Zhao, Y. Cui, J. Chang, Nanomaterials. 14 (2024) 1802. https://doi.org/10.3390/nano14221802

[11] D. Chen, Y. Cheng, N. Zhou, P. Chen, Y. Wang, K. Li, S. Huo, P. Cheng, P. Peng, R. Zhang, L. Wang, H. Liu, Y. Liu, R. Ruan, J. Clean. Prod. 268 (2020) 121725. https://doi.org/10.1016/j.jclepro.2020.121725

[12] Pi, Atkowska, M. Janus, K. Szymá Nski, S. Mozia, Catalysts. 11 (2021) 144. https://doi.org/10.3390/catal11010144

[13] R. Cheng, J. Xia, J. Wen, P. Xu, X. Zheng, Nanomaterials. 12 (2022) 1335. https://doi.org/10.3390/nano12081335

[14] M. Jiang, K. Nozaki, T. Mokudai, Y. Nakano, M. Uo, K. Yamashita, S. Ohara, N. Wakabayashi, ACS Appl. Nano. Mater. 8 (2025) 11568–11581. https://doi.org/10.1021/acsanm.5c01768

[15] A.S.S. Bilal, G. Rodríguez-Ortiz, M. Shahid, S. Ballal, H. Hassan, A. Vashisht, N. Banik, T. Eshchanov, B. Madaminov,

M.U.A. Khan, R. Fatima, Results. Chem. 17 (2025) 102561. https://doi.org/10.1016/j.rechem.2025.102561

[16] W. Navarra, I. Ritacco, O. Sacco, L. Caporaso, M. Farnesi Camellone, V. Venditto, V. Vaiano, J. Phys. Chem. C. 126 (2022) 7000–7011 https://doi.org/10.1021/acs.jpcc.2c00152

[17] N. Omrani, A. Nezamzadeh-Ejhieh, Sep. Purif. Technol. 235 (2020) 116228. https://doi.org/10.1016/j.seppur.2019.116228

[18] S. Ghattavi, A. Nezamzadeh-Ejhieh, Int. J. Hydrogen Energy 45 (2020) 24636–24656. https://doi.org/10.1016/j.ijhydene.2020.06.207

[19] V.U. Siddiqui, A. Ansari, M.T. Ansari, M.K. Akram, W.A. Siddiqi, A.M. Alosaimi, M.A. Hussein, M. Rafatullah, Catalysts. 11 (2021) 1509. https://doi.org/10.3390/catal11121509

[20] H. Dihom, R.M.S.R. Mohamed, A. Al-Gheethi, W.A.B.W. Mohamed, Water Pract. Technol. 19 (2024) 2279–2305. https://doi.org/10.2166/wpt.2024.132

[21] M.K. Lanjewar, O.K. Mahadwad, P. Patil, Iran. J. Catal. https://doi.org/10.57647/ijc.2026.1601.05

[22] M. Rezaei, A.A. Ensafi, E. Heydari-Bafrooei, J. Ind. Eng. Chem. 146 (2025) 589–602. https://doi.org/10.1016/j.jiec.2024.11.043

[23] N. Omrani, A. Nezamzadeh-Ejhieh, Iran. J. Catal.15 (2025) 152515–152516. https://doi.org/10.57647/j.ijc.2025.1502.15

[24] R. Ahmadiasl, G. Moussavi, S. Shekoohiyan, F. Razavian, Catalysts. 12 (2022) 1310. https://doi.org/10.3390/catal12111310

[25] M. Mersal, A.F. Zedan, G.G. Mohamed, G.K. Hassan, Sci Rep. 13 (2023) 1–15. https://doi.org/10.1038/s41598-023-31625-5

[26] X. He, T. Kai, P. Ding, Springer Int. Publ. 19 (2021) 4563-4601. https://doi.org/10.1007/s10311-021-01295-8

[27] S. Khammarnia, H. Hassani, Iran. J. Catal.15 (2025) 152514–152515. https://doi.org/10.57647/j.ijc.2025.1502.14

[28] V. Thongpool, A. Phunpueok, S. Jaiyen, T. Sornkwan, Results Phys. 16 (2020) 102948. https://doi.org/10.1016/j.rinp.2020.102948

[29] H. Derikvandi, M. Vosough, A. Nezamzadeh-Ejhieh, Environ. Sci. Pollut. Res. 27 (2020) 27582–27597. https://doi.org/10.1007/s11356-020-08817-x

[30] P.L. Meena, A.K. Surela, L.K. Chhachhia, J. Meena, R. Meena, Nanoscale Adv. 7 (2025) 1335–1352. https://doi.org/10.1039/d4na00890a

[31] Q. Chen, A. Ozkan, B. Chattopadhyay, K. Baert, C. Poleunis, A. Tromont, R. Snyders, A. Delcorte, H. Terryn, M.P. Delplancke-Ogletree, Y.H. Geerts, F. Reniers, Langmuir. 35 (2019) 7161–7168. https://doi.org/10.1021/acs.langmuir.9b00784

[32] A.B. Anik, M. Hossen Akash, M.A. Alam, M.Z. Alam, D. Sarker, N. Sultana, RSC Adv. 15 (2025) 45874–45888. https://doi.org/10.1039/d5ra06656e

[33] N. Nazari, M.M. Golzan, K. Mabhouti, Sci. Rep. 14 (2024) 6407. https://doi.org/10.1038/s41598-024-57045-7

[34] A.K.M.A. Habib, K.M.R. Rifat, M.E. Kabir, J.N. Khan, S.M.N. Rokon, M.A. Rabbi, Results Mater. 22 (2024) 100581. https://doi.org/10.1016/j.rinma.2024.100581

[35] V. Thongpool, A. Phunpueok, S. Jaiyen, T. Sornkwan, Results Phys. 16 (2020) 102948. https://doi.org/10.1016/j.rinp.2020.102948

[36] S. Sharafzadeh, J. Zolgharnein, A. Nezamzadeh-Ejhieh, S. Dermanaki Farahani, Surf. Interfaces 59 (2025) 105917. https://doi.org/10.1016/j.surfin.2025.105917

[37] B.A. Lemecho, F.K. Sabir, D.M. Andoshe, N.S. Gultom, D.H. Kuo, X. Chen, E. Mulugeta, T.D. Desissa, O.A. Zelekew, Bioinorg. Chem. Appl. 2022 (2022) 1-10. https://doi.org/10.1155/2022/8081494

[38] Z. Zhao, A.A. Omer, Z. Qin, S. Osman, L. Xia, R.P. Singh, Environ. Sci. Pollut. Res. 27 (2020) 17530–17540. https://doi.org/10.1007/s11356-019-05787-7

[39] Y.T. Gaim, G.M. Tesfamariam, G.Y. Nigussie, M.E. Ashebir, J. Compos. Sci. 3 (2019) 93. https://doi.org/10.3390/jcs3040093

[40] S. Krishnan, A. V. Karim, A. Shriwastav, Water Sci. Technol. 86 (2022) 1527–1539. https://doi.org/10.2166/wst.2022.266

[41] Y.S. Kurniawan, L. Yuliati, Bull. Chem. React. Eng. Catal. 16 (2021) 310–319. https://doi.org/10.9767/bcrec.16.2.10319.310-319

[42] Negi, S. Ringwal, M. Pandey, M. Taha Yassin, Sci. Rep. 14 (2024) 7955. https://doi.org/10.1038/s41598-024-57392-5

[43] S.B. Deshmukh, K.H. Deshmukh, M.L. Mane, D. V. Mane, Macromol. Symp. 400 (2021) 2100071. https://doi.org/10.1002/masy.202100071

[44] T.T. Khan, G.A.K.M. Rafiqul Bari, H.J. Kang, T.G. Lee, J.W. Park, H.J. Hwang, S.M. Hossain, J.S. Mun, N. Suzuki, A. Fujishima, J.H. Kim, H.K. Shon, Y.S. Jun, Catalysts. 11 (2021) 1–13. https://doi.org/10.3390/catal11010109

[45] R.T. Konatu, D.D. Domingues, R. França, A.P.R. Alves, J. Funct. Biomater. 14 (2023) 353. https://doi.org/10.3390/jfb14070353

[46] Y. Sun, Y. Gao, B. Zhao, S. Xu, C. Luo, Q. Zhao, Mater. Res. Express. 7 (2020) 085010. https://doi.org/10.1088/2053-1591/abaea4

[47] N. Mintcheva, S. Yamaguchi, S.A. Kulinich, Materials. 13 (2020) 719. https://doi.org/10.3390/ma13030719

[48] K. Prajapat, U. Mahajan, M. Dhonde, K. Sahu, P. Sakthivel, S. Vyas, P.M. Shirage, Mater. Adv. 6 (2025) 2371–2384. https://doi.org/10.1039/d4ma01297f

[49] J.A. Rengifo-Herrera, P. Osorio-Vargas, C. Pulgarin, J. Hazard Mater. 425 (2022) 127979. https://doi.org/10.1016/j.jhazmat.2021.127979

[50] T.S. Natarajan, V. Mozhiarasi, R.J. Tayade, Photochem. 1 (2021) 371–410. https://doi.org/10.3390/photochem1030024

[51] Aadnan, O. Zegaoui, A. El, H. Moussout, J.C.G. Esteves, Arab. J. Chem. 17 (2024) 105336. https://doi.org/10.1016/j.arabjc.2023.105336

[52] M. Elias, M.N. Uddin, J.K. Saha, M.A. Hossain, D.R. Sarker, S. Akter, I.A. Siddiquey, J. Uddin, Molecules. 26 (2021) 1470. https://doi.org/10.3390/molecules26051470

[53] M.T. Uddin, M.E. Hoque, M. Chandra Bhoumick, RSC Adv. 10 (2020) 23554–23565. https://doi.org/10.1039/d0ra03233f

[54] M. Rezaei, A. Nezamzadeh-Ejhieh, A.R. Massah, Energy and Fuels. 38 (2024) 8406–8436. https://doi.org/10.1021/acs.energyfuels.4c00160

[55] M. Rezaei, A. Nezamzadeh-Ejhieh, A.R. Massah, ACS Omega. 9 (2024) 6093–6127. https://doi.org/10.1021/acsomega.3c07560

[56] O. Sacco, A. Mancuso, V. Venditto, S. Pragliola, V. Vaiano, Catalysts. 12 (2022) 1208. https://doi.org/10.3390/catal12101208

[57] S. Sharafzadeh, J. Zolgharnein, A. Nezamzadeh-Ejhieh, S.D. Farahani, Int. J. Hydrogen Energy 106 (2025) 1429–1442. https://doi.org/10.1016/j.ijhydene.2025.02.031

[58] H.D. Tran, D.Q. Nguyen, P.T. Do, U.N.P. Tran, RSC Adv. 13 (2023) 16915–16925. https://doi.org/10.1039/d3ra01970e

[59] Yousefi, A. Nezamzadeh-Ejhieh, Iran. J. Catal. 11 (2021) 247-259. https://oiccpress.com/ijc/article/view/3600

[60] W. Bahnemann, V.K. Landge, C.-M. Huang, V.S. Hakke, S.H. Sonawane, S. Manickam, M.-C. Hsieh, Catalysts 12 (2022) 605. https://doi.org/10.3390/catal12060605

[61] S. Yang, T. Wu, K. Li, P. Huang, W. Li, Y. Zhuo, K. Liu, Z. Yang, D. Han, Molecules 29 (2024) 5418. https://doi.org/10.3390/molecules29225418

[62] Y. Zhang, X. Bo, T. Zhu, W. Zhao, Y. Cui, J. Chang, Nanomaterials 14 (2024) 1802. https://doi.org/10.3390/nano14221802

[63] D.C. Ashiegbu, H.J. Potgieter, Heliyon 9 (2023) e20674. https://doi.org/10.1016/j.heliyon.2023.e20674

[64] M. Malik, S.M. Ibrahim, M.A. Nazir, A.A. Tahir, M.K. Tufail, S.S.A. Shah, A. Anum, M.A. Wattoo, A. ur Rehman, Catalysts 13 (2023) 813. https://doi.org/10.3390/catal13050813

[65] N. Ahmia, M. Benamira, L. Messaadia, H. Lahmar, M. Trari, I. Avramova, Mater. Sci. Eng. B 322 (2025) 118626. https://doi.org/10.1016/j.mseb.2025.118626

[66] N.Y. Donkadokula, A.K. Kola, D. Saroj, Sustain. Environ. Res. 30 (2020) 9. https://doi.org/10.1186/s42834-020-00050-y

[67] V. Gadore, A.K. Singh, S.R. Mishra, M. Ahmaruzzaman, Sci. Rep. 14 (2024) 1118. https://doi.org/10.1038/s41598-024-51618-2

[68] M. Berkani, M.K. Bouchareb, M. Bouhelassa, Y. Kadmi, Top. Catal. 63 (2020) 964–975. https://doi.org/10.1007/s11244-020-01320-0

[69] L. Montazerghaem, M. Keramatifarhodbonab, A. Naeimi, Heliyon. 10 (2024) e24789. https://doi.org/10.1016/j.heliyon.2024.e24789

[70] K. Nelson, A.C. Mecha, A. Kumar, Discover Chem. Eng. 4 (2024) 34. https://doi.org/10.1007/s43938-024-00072-7

[71] H. Ashebir, S. Babaee, A. Worku, P. Diale, T. Msagati, J.F. Nure, Sci. Rep. 15 (2025) 31795. https://doi.org/10.1038/s41598-025-03330-y

[72] S. Sharafzadeh, A. Nezamzadeh-Ejhieh, J. Zolgharnein, Chem. Phys. Impact 11 (2025) 100963. https://doi.org/10.1016/j.chphi.2025.100963

Appendix

Sr. No.	Photocatalyst	Band Gap (Eg), eV	Remark
1	Pure TiO_2	3.19	Mentioned in previous published work and reference given in the present work. [21]
2	Pure ZnO	3.308	
3	Pure ZnO/TiO_2	3.23	
4	7% Cu:ZnO/TiO_2	3.0	
5	7% Cu-N:ZnO/TiO_2	2.97	Present Work

10.57647/ijc.2026.1602.17